

# Geophysical Research Letters®



## RESEARCH LETTER

10.1029/2024GL112851

## Xenolith Constraints on the Mantle Potential Temperature and Thickness of Cratonic Roots Through Time

Z. J. Sudholz<sup>1</sup>  and A. Copley<sup>1</sup> 

<sup>1</sup>Bullard Labs, Department of Earth Sciences, University of Cambridge, Cambridge, UK

### Key Points:

- Pressure and temperature estimates for 7,303 mantle xenoliths and xenocrysts were used to constrain the thermal structure of the lithosphere
- Paleogeotherms with higher mantle  $T_p$  have artificial gaps between the base of the lithosphere and deepest xenoliths and xenocrysts
- Modeled and observed pressures and temperatures of the base of the lithosphere are similar when a mantle  $T_p$  of 1,315°C is used

### Supporting Information:

Supporting Information may be found in the online version of this article.

### Correspondence to:

Z. J. Sudholz,  
zs441@cam.ac.uk

### Citation:

Sudholz, Z. J., & Copley, A. (2025). Xenolith constraints on the mantle potential temperature and thickness of cratonic roots through time. *Geophysical Research Letters*, 52, e2024GL112851. <https://doi.org/10.1029/2024GL112851>

Received 2 OCT 2024  
Accepted 16 DEC 2024

### Author Contributions:

**Conceptualization:** Z. J. Sudholz, A. Copley  
**Methodology:** Z. J. Sudholz, A. Copley  
**Writing – original draft:** Z. J. Sudholz, A. Copley  
**Writing – review & editing:** Z. J. Sudholz, A. Copley

**Abstract** The temperature of the convecting mantle and thickness of the lithosphere control many of Earth's processes. However, there is disagreement regarding the evolution of these quantities through time. We use a global data set of mantle xenoliths and xenocrysts to construct paleogeotherms at different eruption ages (16–1,311 Ma) and estimate the temperature and depth of the lithosphere-asthenosphere boundary (LAB) as a function of mantle potential temperature ( $T_p$ ). We find that the maximum pressure and temperature (PT) of xenoliths matches the modeled LAB conditions when a  $T_p$  of 1,315°C is used. At higher  $T_p$  (1,450–1,550°C) we observe a gap between the maximum PT of xenoliths and the LAB conditions. Because this gap systematically increases with  $T_p$ , and the maximum PT of xenoliths has not changed over time, we suggest that there has actually been only minor (<50°C) changes in mantle  $T_p$  since the Meso-Proterozoic.

**Plain Language Summary** The temperature of the convecting mantle and the thickness of the lithosphere control many of Earth's processes. There is disagreement as to whether the temperature of the convecting mantle and thickness of the lithosphere were greater during Earth's early history. In this study we address this issue by using a global data set of mantle xenoliths and xenocrysts. Xenolith pressure and temperature (PT) estimates are used to construct paleogeotherms at different eruption ages and values for mantle potential temperature ( $T_p$ ) to constrain the conditions of the lithosphere-asthenosphere boundary (LAB). PT estimates are compared with the LAB conditions at different eruption ages and mantle  $T_p$  values. We find that the maximum PT of the samples are similar to the conditions of the LAB when a present day  $T_p$  is used ( $T_p = 1,315^\circ\text{C}$ ). Models that use a higher  $T_p$  (1,450–1,550°C) result in large gaps between the LAB and the maximum PT of xenoliths and xenocrysts. The size of the gaps increase systematically with higher values for  $T_p$ . This, along with the observation that the maximum PT of xenoliths and xenocrysts has not changed over time, suggests that  $T_p$  and lithospheric thickness were not significantly greater during the Proterozoic.

## 1. Introduction

Secular changes in the temperature of the convecting mantle and the thickness of the continental lithospheric mantle (CLM) have been widely debated. These properties are of interest because they influence the stability and evolution of continents (Lenardic et al., 2003; McKenzie & Priestley, 2008), the volume and composition of mantle-derived melts (Ganne & Feng, 2017; Herzberg et al., 2007, 2010), the formation and distribution of ore deposits (Gibson et al., 2024; Hoggard et al., 2020), and the geodynamics of the lithosphere (Korenaga, 2006, 2018; Weller et al., 2019). Specifically, there has been long-standing debate as to whether the temperature of the convecting mantle, which sets the temperature at the lithosphere-asthenosphere boundary (LAB), and the thickness of the CLM were greater during the Precambrian than at the present day.

Evidence for secular cooling of the convecting mantle since the Archean has come from three main data sets. (a) The formation of komatiites during the Precambrian has long been considered as primary evidence for a hotter convecting mantle during this period (Herzberg et al., 2007, 2010). Komatiites are anomalously hot lavas that have a temporal and spatial affinity to cratons. Experimental and petrological studies have shown that komatiites form at high temperatures (>1,500°C) by high-degree partial melting of peridotite (Walter, 1998). With the exception of several occurrences, these conditions have been absent during the Phanerozoic (Grove & Parman, 2004). Modeling of komatiite and basalt compositions suggests that the potential temperature of the mantle ( $T_p$ ) (the temperature that the solid adiabatically convecting mantle would have if it could reach the surface metastably without melting; McKenzie & Bickle, 1988) during the Precambrian may have been up to 400°C higher than present day ( $T_p \cong 1,315^\circ\text{C}$ ) (Herzberg et al., 2007, 2010). (b) A second line of evidence has come from the use of Urey ratios (the ratio of internal heat production to surface heat flux) to calculate mantle  $T_p$  back

© 2025. The Author(s).

This is an open access article under the terms of the [Creative Commons Attribution License](https://creativecommons.org/licenses/by/4.0/), which permits use, distribution and reproduction in any medium, provided the original work is properly cited.

through time (Herzberg et al., 2010; Korenaga, 2008b). At lower Urey ratios (0.21–0.38), secular trends in  $T_p$  show an increase from  $\sim 1,315^\circ\text{C}$  at present day to  $\sim 1,575\text{--}1,650^\circ\text{C}$  at  $\sim 2.5$  Gyr. These results have been suggested to agree with secular cooling trends from komatiites and basalts (Herzberg et al., 2010). If this temperature range is correct, the maximum thickness of cratons may have exceeded  $>400$  km during the Precambrian (Ballard & Pollack, 1987, 1988; Hoare et al., 2022). (c) Finally, evidence has also come from diamond inclusions and mantle-derived xenoliths (Hoare et al., 2022; Kamber & Tomlinson, 2019). Some data sets have recorded elevated PT estimates relative to present day ( $>1,500^\circ\text{C}$  and  $>8$  GPa), and/or steeper reconstructed paleo-geothermal gradients that intersect the mantle adiabat at greater depths, particularly when a higher value for  $T_p$  is considered (Hoare et al., 2022). These observations have been used to infer CLM thicknesses of up to 400 km during the Precambrian (Hoare et al., 2022; Kamber & Tomlinson, 2019).

Contrasting evidence suggesting that the temperature of the convecting mantle and thickness of the CLM has not changed significantly has come from three data sets. (a) Inferred lithospheric thicknesses of up to 400 km during the Precambrian differ substantially from present day values from seismic tomography (Priestley et al., 2024). Although delamination and thermal-mechanical erosion could be responsible for the removal of part of the CLM (Bird, 1979; Fan et al., 2000) there remains little evidence that these mechanisms have operated continuously since the Precambrian beneath all cratons. Estimates of present-day CLM thickness from seismology are also in close agreement with paleogeotherms for Phanerozoic and Proterozoic xenolith suites (Hoggard et al., 2020; Sudholz et al., 2022, 2023). (b) The significance of komatiites and basalts in secular cooling models for Earth have been widely discussed. Some authors suggest that there is little evidence for secular change in the MgO concentration of these rocks, particularly during the Archean (Campbell & Griffiths, 2014; Kamber, 2010; Kamber & Tomlinson, 2019), and that basaltic magmas have persisted through geological time with similar mean MgO content as far back as the Paleoproterozoic (Kamber, 2015). Additionally, some models using komatiites and basalts (Ganne & Feng, 2017; Keller & Schoene, 2018) suggest that  $T_p$  has only cooled slightly ( $\leq 200^\circ\text{C}$ ) since 2.5 Gyr. The role of higher  $T_p$  in komatiite petrogenesis forms the cornerstone for many ‘hot early Earth’ models. However, several studies have shown that they may also form in comparatively cooler mantle settings. For example, McKenzie (2020) demonstrated that komatiites can form by relatively low-degree partial melting at the base of the upper mantle and be transported in plumes no more than  $\sim 50^\circ\text{C}$  hotter than present-day examples. Further, several studies have suggested that komatiites can also form by shallow-level wet-melting above subduction zones (Grove & Parman, 2004). (c) Finally, there is considerable uncertainty over the use of Urey ratios in defining thermal evolution trends for Earth, both in terms of the value at the present day (Davies, 2009; Korenaga, 2008a, 2008b; Lenardic et al., 2011), and the likelihood that it has changed through time (Jaupart et al., 2007).

Despite decades of research there is still disagreement as to whether the temperature of the convecting mantle and the thickness of the CLM were greater during the Precambrian. In this study we address this issue using mantle xenoliths, xenocrysts, and diamond inclusions hosted in kimberlites and related rocks. We use the equilibration pressures and temperatures (PT) of these samples, in conjunction with paleogeotherm models, to constrain the PT conditions of the LAB through time as a function of  $T_p$  and eruption age. Our results have important implications for developing and interpreting geodynamic models of early Earth and for understanding temporal and spatial changes in past and present Earth processes.

## 2. Mantle Xenolith Data Set

Mantle xenoliths and xenocrysts are the products of sampling of the lithospheric mantle by rapidly ascending magmas such as kimberlites (Pearson et al., 2003). Xenoliths and xenocrysts provide snapshots of the composition and lithology of the CLM at the time of eruption. When used in conjunction with geothermobarometers and paleogeotherm models, they can be used to constrain the temperature and thickness of the CLM at the time of eruption, including the temperature of the LAB. To study the spatial and temporal changes in the temperature and thickness of the lithosphere we have compiled a published global data set of xenoliths and xenocrysts (Figure 1). Our data set includes samples from most cratons and covers host-rock eruption ages from the Miocene to Paleoproterozoic. We analyze the chemical concentrations of major and minor oxides in clinopyroxene, because it is an abundant mineral in the CLM and can be used to calculate the equilibration PT at the time of eruption. We obtain these PT conditions using single-grain geothermobarometry, which can be applied to large suites of disaggregated xenoliths where key geothermobarometric phases such as olivine and orthopyroxene may be absent. The application of single-grain clinopyroxene geothermobarometry to experimental and natural data sets is

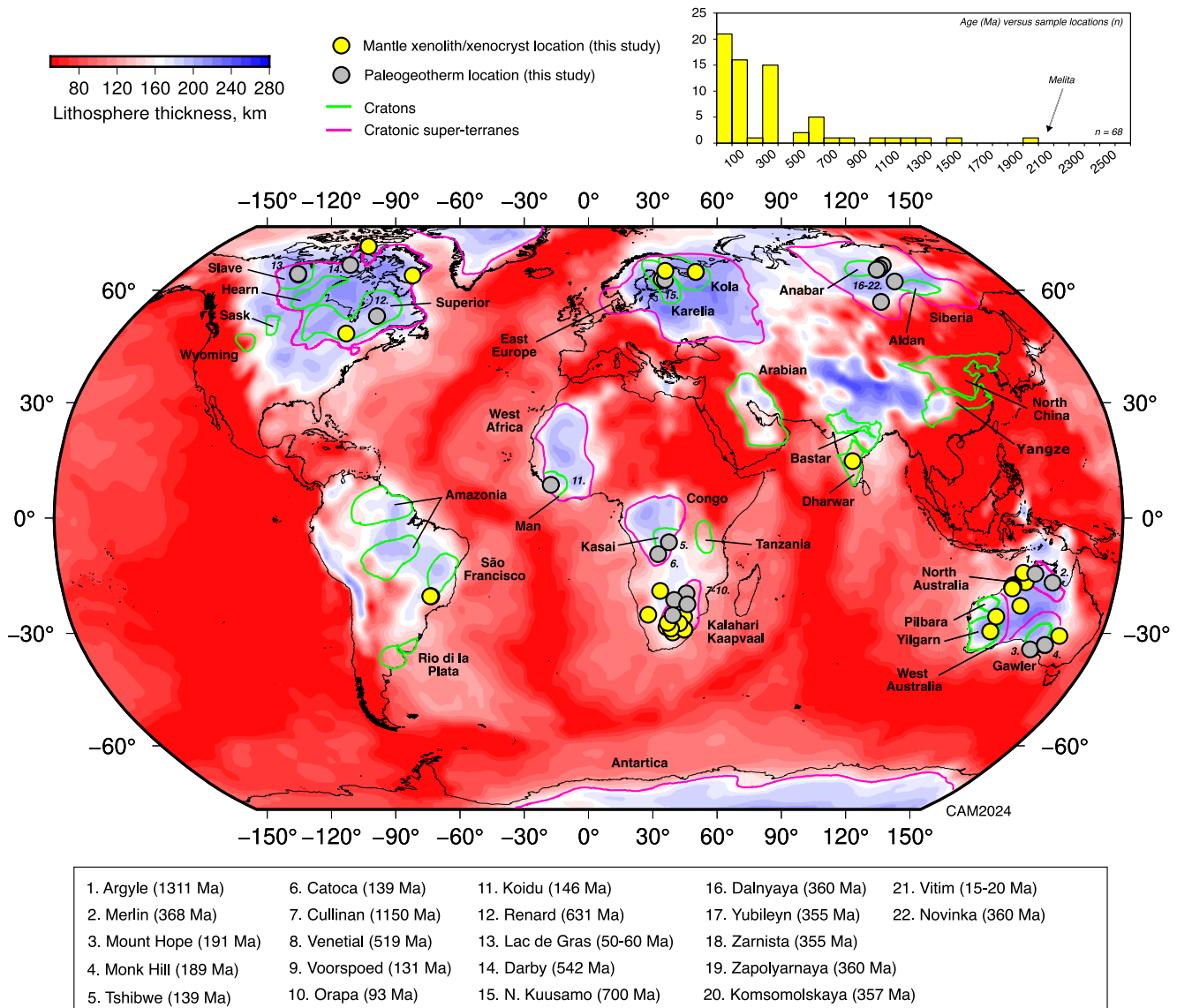


**Figure 1.** Summary of the mantle xenolith and xenocryst locations used in this study overlain on the modeled global lithosphere thickness (CAM2024; Priestley et al., 2024). Symbols for mantle xenoliths and xenocrysts includes our global compilation of samples as well as the sample locations used for paleogeotherm modeling (see Methods). Also shown is the approximate outlines of cratonic lithosphere and cratonic super-terranes. The emplacement ages of mantle xenolith and xenocrysts are expressed in a histogram (top-right) (BIN = 100 Myr). Refer to the supplementary file for the emplacement ages of the samples and details on the samples and references.

well documented and the sources of errors are understood (Nimis & Grütter, 2010; Zibera et al., 2016). Clinopyroxene compositions were typically measured using an electron probe microanalyzer. To ensure a consistent level of data-quality we have excluded clinopyroxenes with major and minor oxide totals outside of the range 98–102 wt% and cation normalized totals outside of the range of 3.98–4.02 cations per formula unit. The equilibration PT of clinopyroxenes were determined using the single-grain Cr-in-clinopyroxene geobarometer and enstatite-in-clinopyroxene geothermometer (Nimis & Taylor, 2000; Sudholz et al., 2021). The geothermobarometer is suitable for clinopyroxenes that equilibrated with garnet and orthopyroxene in a peridotitic source. To ensure equilibration with these phases we have applied the filtering method of Zibera et al. (2016). Our final data set contained 7,303 clinopyroxenes.

### 3. Paleogeotherm Modeling

Because kimberlites and related volcanic rocks form by low degree partial melting within the convecting mantle or near the lithosphere-asthenosphere boundary (Foley et al., 2019; Tappe et al., 2018), xenoliths can sample PT conditions over large depth ranges within the lithospheric mantle. Constructing paleogeotherms to reproduce these PT estimates provides a method to assess secular changes in the thermal structure of the lithosphere, including the conditions of the LAB. Paleogeotherms were constructed using a method based upon McKenzie et al. (2005), which is also the method used by FITPLOT (Mather et al., 2011). Rather than fix the values of poorly known parameters (crustal thickness in the past, heat production rates,  $T_p$ ), we instead calculate many paleogeotherms spanning wide ranges of geologically plausible input parameters and count all models as ‘successful’ that reproduce the PT estimates to within a specified tolerance (typically root mean square (RMS) misfits to the entire data set for each locality of  $<60\text{--}75^\circ\text{C}$ ). We then analyze the parameters of all successful models (Supporting Information S1). We only apply this technique to a subset of our PT estimates, which are from individual localities ( $n = 22$ ) that sample a wide enough range of P conditions to allow well-constrained paleogeotherms to be produced. Our RMS misfit approach excludes xenolith suites that have experienced significant pre-eruption thermal perturbations (e.g., Liu et al., 2022), because these do not plot along a conductive geotherm and so result in misfits above our cut-off level. Additionally, we exclude any locations where visual inspection reveals thermal perturbations, expressed as a noticeable skew in PT determinations away from a conductive geotherm (such as Cullinan (Nimis et al., 2020), Ashmore (Sudholz et al., 2023), and Udachnaya (Liu et al., 2022), where thermally perturbed samples form arrays sub-parallel to the mantle isentrope).

The paleogeotherm models allow us to estimate the temperature throughout the lithosphere based upon our (varied) input parameters, which are the thicknesses and radiogenic heating rates of the upper and lower crust, and the heat flux through the lithospheric mantle (example paleogeotherms are shown on Figure 2). The conditions at the base of the lithosphere for each model can be estimated by examining where the successful paleogeotherms intersect mantle isentropes calculated for a range of values of  $T_p$  (i.e., the intersection of the paleogeotherms with the dashed lines on Figure 2). We use a range of values of  $T_p$ , constructed by varying  $dT/dt$  ( $^\circ\text{C Gyr}^{-1}$ ), where  $T$  is the mantle  $T_p$ , and  $t$  is age in Gyr, and cooling through time is defined as positive values. Five values for  $dT/dt$  were considered:  $dT/dt = 0, 25, 50, 75,$  and  $100^\circ\text{C Gyr}^{-1}$ . Models using a  $dT/dt$  of  $0^\circ\text{C Gyr}^{-1}$  have a  $T_p$  that does not change through time from the present day value of  $T_p = 1,315^\circ\text{C}$ . Conversely, models using a  $dT/dt$  of  $100^\circ\text{C Gyr}^{-1}$  have a  $T_p$  that changes by  $100^\circ\text{C}$  per Gyr, such that at 2 Gyr the  $T_p = 1,515^\circ\text{C}$ , equivalent to the estimates of Herzberg et al. (2010) and Korenaga (2008b). Using a linear change in  $T_p$  through time is an acceptable approximation to curves calculated from the Urey ratio approach for the time interval over which the xenoliths erupted ( $<1.3$  Ga). The  $T_p$  values used in the calculations at the time of eruption for each location were calculated using the different values for  $dT/dt$  and published geochronological data for eruption age (Supporting Information S1; Sudholz & Copley, 2024).

An example model result is shown for the 1.3 Ga Argyle lamproite on Figure 2. The successful paleogeotherms calculated using a range of input parameters are shown as gray lines on Figure 2a. The paleogeotherms encompass all successful models that fit the xenolith and xenocryst PT data with an RMS misfit of  $<60^\circ\text{C}$ . The ranges in crustal thickness for the successful models are shown as histograms on Figures 2b and 2c. Additionally, the ranges in heat production ( $\mu\text{ Wm}^{-3}$ ) within the upper and lower crust are shown on Figures 2d and 2e respectively. The successful values of the heat flux through the lithospheric mantle are shown in Figure 2f. We also illustrate the difference in temperature (T-gap) and pressure (P-gap) between the highest xenolith T and P estimates and the modeled LAB conditions, as a function of  $dT/dt$  and using the eruption age of  $\sim 1.3$  Gyr (Figures 2g–2n).

### 4. Results and Conclusions

PT estimates of our global xenolith and xenocryst data set span 2.0–8.4 GPa and  $453\text{--}1,449^\circ\text{C}$ , and are summarized on Figure 3a. The maximum PT values are similar to estimates using other geothermobarometers (Nickel & Green, 1985; Taylor, 1998). The similarity suggests that mantle xenoliths and xenocrysts record similar equilibration pressures and temperatures within the mantle, and that our geothermobarometer choice has not inadvertently biased the PT range. The range in PT estimates are similar for all sample types (mantle xenoliths, single-grain xenocrysts and diamond inclusions; Figure 3a). This similarity suggests that diamond inclusions did not equilibrate in an anomalously thicker or hotter mantle setting, which is an important observation because previous studies (Hoare et al., 2022) have suggested that the PT estimates of diamond inclusions may record

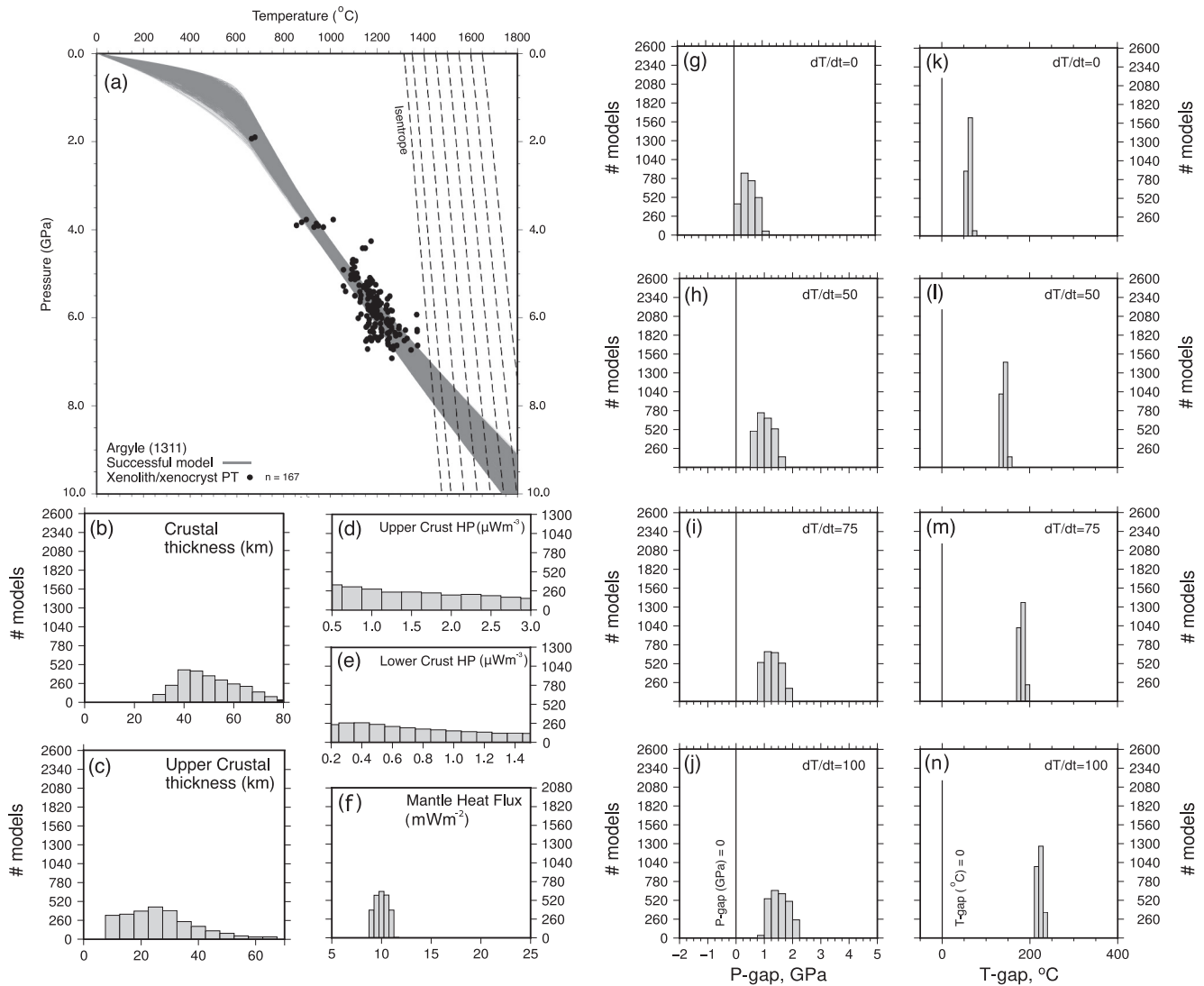


**Figure 2.** Summary of the paleogeotherm model for Argyle (1.3 Gyr). (a) Successful paleogeotherm models (gray lines) that fit xenolith and xenocryst PT estimates (black circles). Dashed lines are mantle isentropes calculated using  $T_p = 1,315^\circ\text{C}$  (lowest line), and then at intervals of  $50^\circ\text{C}$  from  $1,350^\circ\text{C}$  to  $1,650^\circ\text{C}$ . Histograms of the range in total crustal thickness (b) and upper crustal thickness (c) (both km) for successful paleogeotherm models. In all histograms, the y-extent corresponds to the total number of successful models. Histograms of the range in upper (d) and lower (e) crustal heat production (HP) (both  $\mu\text{Wm}^{-3}$ ) for successful paleogeotherm models. Histogram of the mantle heat flux ( $\text{mWm}^{-2}$ ) for successful paleogeotherm models (g)–(j) Histograms of the range in the width of the P-gap for successful paleogeotherm models completed at different values for  $dT/dt$  (refer to Figure legend for  $dT/dt$  value) (k–n) Histograms of the range in the width of the T-gap for successful paleogeotherm models completed at different values for  $dT/dt$  (refer to Figure legend for  $dT/dt$  value).

steeper paleogeotherm gradients thought to be indicative of a thicker Precambrian CLM. The relationship between the equilibration PT and eruption age shows a near horizontal trend through time, becoming sparsely sampled at  $>1.3$  Ga (Figures 3b and 3c). This pattern shows that samples were not sourced from hotter or deeper mantle conditions in the Proterozoic relative to present day. If the CLM had systematically thinned and/or cooled since the Precambrian, it is expected that older xenoliths and xenocrysts would sample higher pressures and temperatures than more recent ones. The consistency in the PT estimates through time is therefore suggestive that there has been a negligible change in the temperature ( $<100^\circ\text{C}$ ) and lithosphere thickness ( $<25$  km) of most cratons since the Proterozoic. We now investigate these findings further using the results of the paleogeotherm modeling. This modeling is used because the thermal gradient within the lithosphere does not, on its own, imply a similar lithosphere thickness and  $T_p$  in the past. To investigate that issue, we compare the xenolith and xenocryst results to the results of the paleogeotherm models, to investigate what values of  $T_p$  and lithosphere thickness are consistent with the observations.

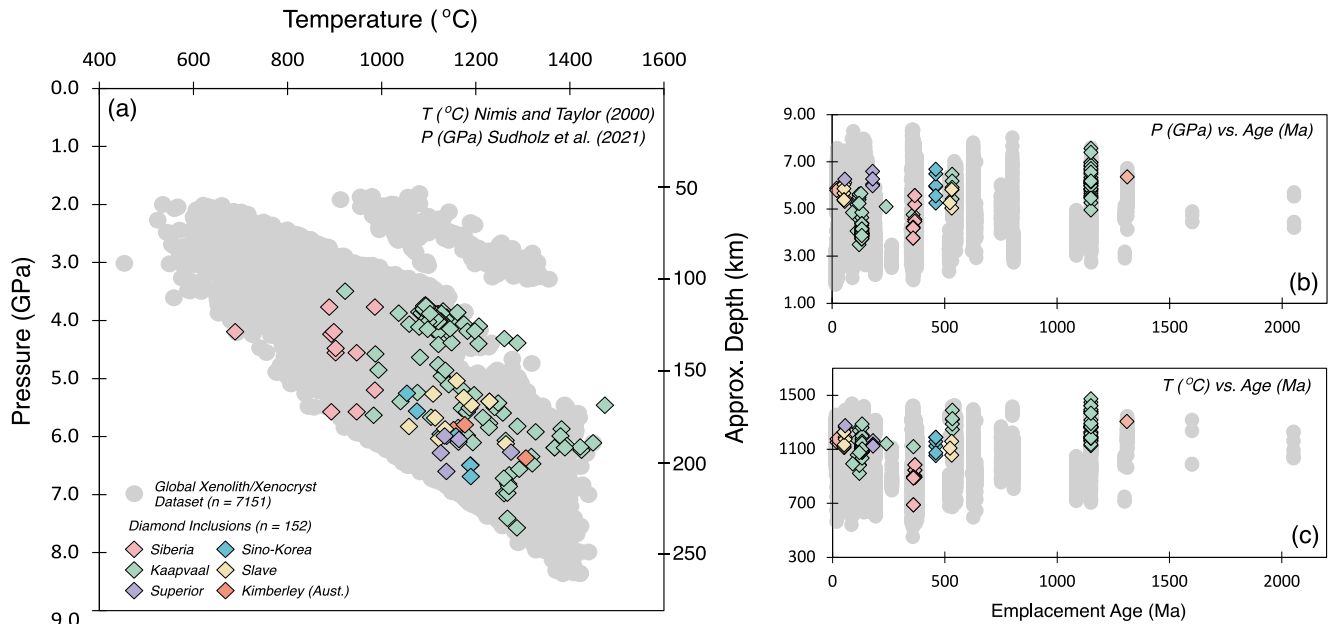


**Figure 3.** Estimates of the PT estimates of mantle xenoliths, xenocrysts and diamond inclusions from a global data set, which passed the filtering processes described in the text. (a) PT estimates of clinopyroxene mantle xenoliths and xenocrysts (gray circles) and clinopyroxene diamond inclusions (diamonds). (b) Relationship between the P of clinopyroxenes and the eruption age of the host rock. (c) Relationship between the T of clinopyroxenes and the eruption age of the host rock.

The range of successful paleogeotherm models for all localities (results equivalent to Figure 2 are presented in Supporting Information S1) show crustal thicknesses between 20 and 80 km, with most models concentrated between 30 and 50 km. This range is similar to seismological estimates at the present day in the cratonic regions where our xenolith suites occur (Szwilius et al., 2019). This similarity is expected given that the generally undeforming nature of these regions would result in limited changes in crustal thickness since the Proterozoic and supports the effectiveness of paleogeotherm modeling. The thickness of the upper crust, and the rates of radiogenic heating in the upper and lower crust, trade-off against each other so are not well constrained. Conversely, the heat flux through the CLM is tightly constrained by the PT estimates and varies between  $\sim 7$  and  $20 \text{ mWm}^{-2}$  (Supporting Information S1), which is similar to published models for the present day (Jaupart et al., 1998; McKenzie et al., 2005).

The relationship between the size of the T-gap and P-gap between the hottest and deepest samples in each locality and the modeled LAB conditions, eruption age (Gyr), and change in  $T_p$  over time ( $dT/dt$ ;  $^{\circ}\text{C Gyr}^{-1}$ ) are summarized on Figure 4. The symbols are the mean T-gap and P-gap for each sample location, determined from the full range of successful paleogeotherms, and the bars show the range covered by the successful models ( $1\sigma$ ). The gray lines show linear fits to the results. Paleogeotherms made using a fixed  $T_p$  of  $1,315^{\circ}\text{C}$  ( $dT/dt = 0^{\circ}\text{C Gyr}^{-1}$ ) show no systematic change in the size of the P-gap (Figure 3a) and T-gap (Figure 3b) with increasing eruption age. The P-gap and T-gap are typically 0–0.7 GPa and 0–50°C. It is likely that these values represent the thickness of, and temperature contrast across, the thermal boundary layer at the base of the lithosphere (Priestley et al., 2024). Our method of estimating LAB conditions by the intersection between a conductive paleogeotherm and a mantle isentrope neglects the existence of this boundary layer, and it is likely that the mantle xenoliths and xenocrysts will not sample this thin region at the base of the plate undergoing small-scale convection.

Paleogeotherm models made using higher values for the change in  $T_p$  through time result in systematic increases in the size of the T-gap and P-gap with increasing eruption age (Figures 3c–3j), indicating a considerable discrepancy between the maximum PT of xenoliths and xenocrysts and the modeled LAB conditions. We interpret this pattern to mean that the  $T_p$  and lithosphere thicknesses in the studied locations have remained roughly constant over the  $\sim 1.3$  Ga time interval over which the xenoliths and xenocrysts had erupted, and that increasing  $T_p$  in the models results in the artificial creation of thick layers of mantle lithosphere that did not exist and are therefore not sampled by the xenoliths and xenocrysts.

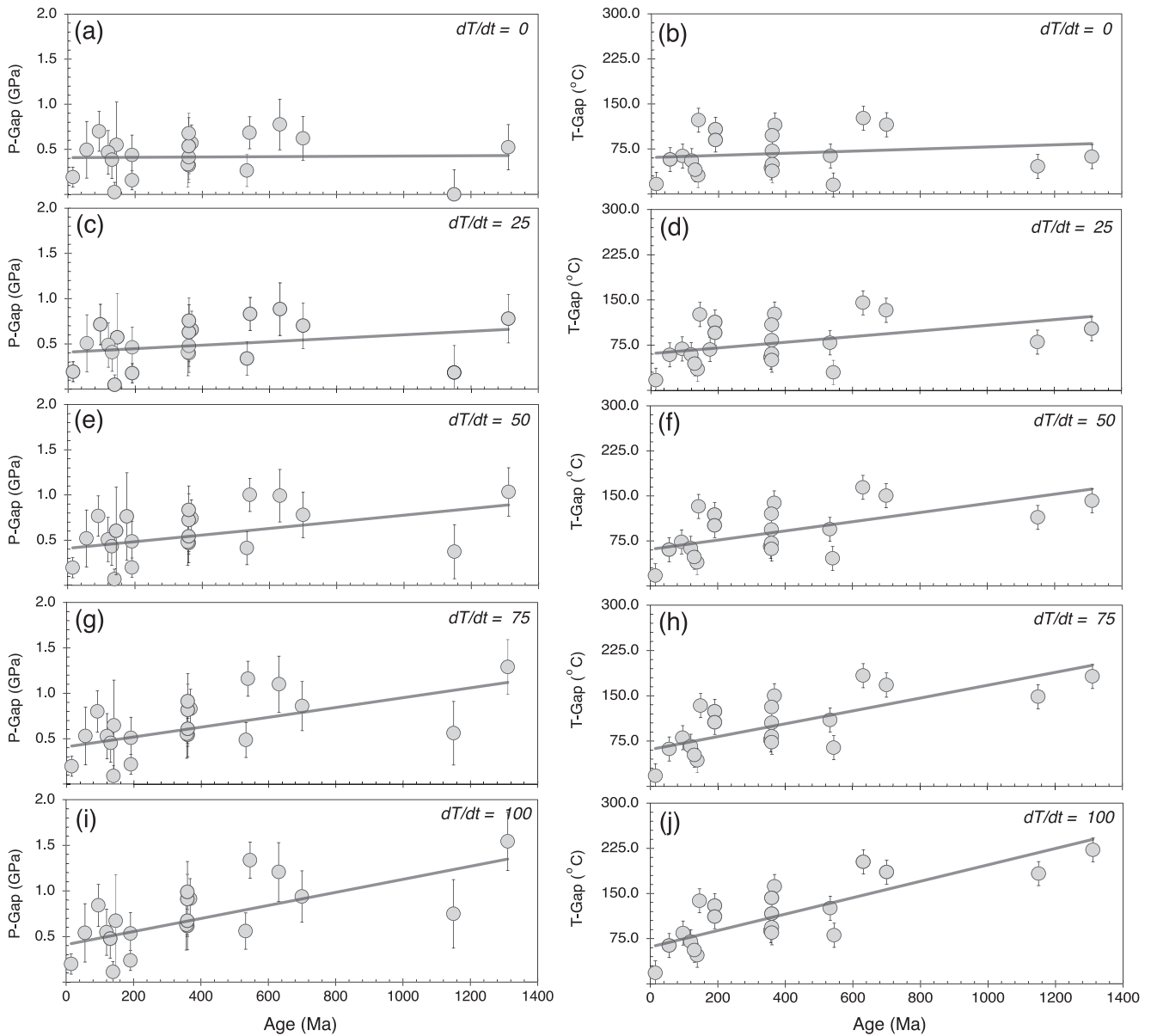


**Figure 4.** The relationship between the size of the T-gap and P-gap between the hottest and deepest xenoliths and xenocrysts in each locality and the modeled LAB conditions, xenolith and xenocryst eruption age, and change in  $T_p$  over time ( $dT/dt$ ;  $^{\circ}\text{C Gyr}^{-1}$ ). Each symbol is a different sample location. The T-gap and P-gap at each location were determined from the paleogeotherm models by calculating the PT difference between the modeled LAB and the average PT of the deepest and hottest xenolith and xenocryst sample at each location (in Supporting Information S1; Sudholz & Copley, 2024).

An alternative suggestion that samples are not recovered from near the base of the lithosphere is inconsistent with the low T- and P-gaps for modern and recent suites, showing that the xenoliths and xenocrysts sample near the LAB. A further alternative that the Proterozoic lithosphere was thicker, but contained a clinopyroxene-absent lower portion, is made unlikely by the difficulty in producing such a melt-depleted layer over a narrow depth range. Additionally, the depth of clinopyroxene depletion would be required to be coincidentally similar to the hypothetical greater thickness of the lithosphere in the past when compared to the present day. The occurrence of a universal clinopyroxene-free layer along the base of the CLM is not supported by global compilations of mantle-derived garnet xenocrysts which show that CaO-depleted varieties are more common within the shallow to middle CLM as opposed to the deeper CLM (Griffin et al., 2003, 2004). These findings are consistent with phase equilibria models for a representative peridotite, KLB-1, which show that the clinopyroxene-out reaction occurs

at  $>1,650^{\circ}\text{C}$  at pressures of  $>5$  GPa (Riel et al., 2022), implying that clinopyroxene is stable throughout the lithosphere in generic compositions, with clinopyroxene-absent assemblages being limited to those that have experienced unusually large amounts of depletion (e.g., Walter, 1998; and the depleted Harzburgite sample BP002 modeled by Tomlinson & Holland, 2021). A final possibility of xenolith and xenocryst extraction not being possible at the depths and temperatures represented by hypothetical thicker Proterozoic craton roots is equally unlikely, given the lack of a dynamic reason why extraction should be possible between  $\sim 2$  and  $7$  GPa and  $\sim 500$ – $1,400^{\circ}\text{C}$  (Figure 3), corresponding to the present-day thickness, but not an additional  $\sim 1$ – $2$  GPa and  $\sim 100$ – $200^{\circ}\text{C}$  beneath that. Such a suggestion implies that there is no cut-off temperature within lithospheric conditions beyond which xenoliths and xenocrysts cannot be extracted from the walls of a melt conduit. Our use of clinopyroxene xenocrysts, which are less dense and easier to entrain in a kimberlite melt in comparison to large multi-mineralic mantle xenoliths, strengthens this assumption, especially given that there is no systematic offset in maximum temperatures between xenoliths and xenocrysts. Additionally, because kimberlites form within the convecting mantle, it is reasonable to assume that entrainment likely commences once these magmas enter the lithosphere, regardless of depth and temperature of the LAB. Finally, comparable PT ranges for different geothermobarometers, and the wider calibration range of our chosen calibration, rules out any possible biases that may result for the methods used for the determination of PT. Therefore, taken together, our results suggest that any changes in  $T_p$  or lithosphere thickness in our studied locations has been irresolvably small,  $<100^{\circ}\text{C}$  and  $<25$  km, since  $\sim 1.3$  Ga. Such an interpretation is also consistent with the lithosphere thicknesses calculated from the xenoliths and xenocrysts using present-day  $T_p$  agreeing with seismological estimates (Priestley et al., 2024, Figure 1).

The absence of mantle xenoliths and xenocrysts erupted before 1.3 Ga that are amenable to the techniques used in this paper places limits on how far back through geological time our results apply. It is known that some amount of secular cooling of the mantle must have occurred, as indicated by the presence of komatiites from the first half of Earth's history (Nesbitt et al., 1982). If the secular cooling was approximately constant through time, then our results indicate that the  $T_p$  in the Archean was likely to have been only up to  $100^{\circ}\text{C}$  hotter than present day. These results are consistent with those of McKenzie (2020), who showed that komatiites can be produced by mantle plumes only  $\sim 50^{\circ}\text{C}$  hotter than those at the present day, and with global compilations which record only slight changes in basalt major oxide compositions since the Proterozoic and Archean (Ganne & Feng, 2017; Keller & Schoene, 2018). We therefore suggest that there have only been modest changes in  $T_p$  through time, or, considerably less likely, that any significant cooling occurred only before  $\sim 1.3$  Ga, by some unknown mechanism that has since ceased to operate.

A wider implication of our results is that there is no significant change in heat flux through the mantle lithosphere as a function of time, since the mid-Proterozoic (see Figure S3 in Supporting Information S1). Reproducing this feature with a different  $T_p$  or lithosphere thickness would require the two parameters to vary in tandem, maintaining a constant heat flux. However, our results above regarding the absence of hot and deep xenoliths or xenocrysts that could be sampling such thicker, hotter, lithosphere shows that the limited range in heat flux is instead due to similar  $T_p$  and lithosphere thicknesses since  $\sim 1.3$  Ga.

A school of models that invoke hot and/or thin lithosphere in the Proterozoic (Roberts et al., 2023; Spencer et al., 2021; Tang et al., 2021) may be relevant to young deformation belts, but our results show that they do not apply to the stable continental interiors sampled by kimberlites that we have studied here. Limited changes in  $T_p$  over the time period we have studied further imply minimal changes in the buoyancy force acting on subducting slabs (Weller et al., 2019), or in the mechanical strength of the continental lithosphere (Copley & Weller, 2024). Between them, these features support conceptual models that invoke minimal changes in the tectonic behavior of the Earth since the mid Proterozoic (Cawood et al., 2018). Furthermore, the minimal variation in  $T_p$  since the mid Proterozoic implies that the Earth's Urey ratio is either high (Herzberg et al., 2010), or perhaps more likely that it changes through time (Jaupart et al., 2007).

### Conflict of Interest

The authors declare no conflicts of interest relevant to this study.

## Data Availability Statement

All geochemical data reported in this study is available from the Zenodo Data Repository under the reference Sudholz and Copley (2024) (10.5281/zenodo.14376664).

## Acknowledgments

Owen Weller, James Jackson, Keith Priestly, Dan McKenzie and Mike Bickle are thanked for discussions on mantle T<sub>p</sub> and related subjects. Paolo Nimis (Padova) is thanked for providing access to his xenolith database. Clinopyroxene diamond inclusions were taken from the Diamond Inclusion Database (maintained by T. Stachel; University of Alberta: <https://cms.eas.ualberta.ca/team-diamond/downloads/>). Francisco Apen and one anonymous reviewer are thanked for their comments. Germán Prieto is thanked for editorial handling. This work was funded by NERC grant NE/W00562X/1.

## References

- Ballard, S., & Pollack, H. N. (1987). Diversion of heat by Archean cratons: A model for southern Africa. *Earth and Planetary Science Letters*, 85(1–3), 253–264. [https://doi.org/10.1016/0012-821x\(87\)90036-7](https://doi.org/10.1016/0012-821x(87)90036-7)
- Ballard, S., & Pollack, H. N. (1988). Modern and ancient geotherms beneath southern Africa. *Earth and Planetary Science Letters*, 88(1–2), 132–142. [https://doi.org/10.1016/0012-821x\(88\)90052-0](https://doi.org/10.1016/0012-821x(88)90052-0)
- Bird, P. (1979). Continental delamination and the Colorado plateau. *Journal of Geophysical Research*, 84(B13), 7561–7571. <https://doi.org/10.1029/jb084ib13p07561>
- Campbell, I. H., & Griffiths, R. W. (2014). Did the formation of D<sup>″</sup> cause the Archaean–Proterozoic transition? *Earth and Planetary Science Letters*, 388, 1–8. <https://doi.org/10.1016/j.epsl.2013.11.048>
- Cawood, P. A., Hawkesworth, C. J., Pisarevsky, S. A., Dhume, B., Capitanio, F. A., & Nebel, O. (2018). Geological archive of the onset of plate tectonics. *Philosophical Transactions of the Royal Society A: Mathematical, Physical & Engineering Sciences*, 376(2132), 20170405. <https://doi.org/10.1098/rsta.2017.0405>
- Copley, A., & Weller, O. M. (2024). Modern-style continental tectonics since the early Archean. *Precambrian Research*, 403, 107324. <https://doi.org/10.1016/j.precamres.2024.107324>
- Davies, G. F. (2009). Effect of plate bending on the Urey ratio and the thermal evolution of the mantle. *Earth and Planetary Science Letters*, 287(3–4), 513–518. <https://doi.org/10.1016/j.epsl.2009.08.038>
- Fan, W. M., Zhang, H. F., Baker, J., Jarvis, K. E., Mason, P. R. D., & Menzies, M. A. (2000). On and off the North China craton: Where is the Archean keel? *Journal of Petrology*, 41(7), 933–950. <https://doi.org/10.1093/petrology/41.7.933>
- Foley, S. F., Yaxley, G. M., & Kjarsgaard, B. A. (2019). Kimberlites from source to surface: Insights from experiments. *Elements: An International Magazine of Mineralogy, Geochemistry, and Petrology*, 15(6), 393–398. <https://doi.org/10.2138/gselements.15.6.393>
- Ganne, J., & Feng, X. (2017). Primary magmas and mantle temperatures through time. *Geochemistry, Geophysics, Geosystems*, 18(3), 872–888. <https://doi.org/10.1002/2016gc006787>
- Gibson, S., McKenzie, D., & Lebedev, S. (2024). The distribution and generation of carbonatites. *Geology*, 52(9), 667–671. <https://doi.org/10.1130/g52i141.1>
- Griffin, W. L., O'Reilly, S. Y., Doyle, B. J., Pearson, N. J., Coopersmith, H., Kivi, K., et al. (2004). Lithosphere mapping beneath the North American plate. *Lithos*, 77(1–4), 873–922. <https://doi.org/10.1016/j.lithos.2004.03.034>
- Griffin, W. L., O'Reilly, S. Y., Natapov, L. M., & Ryan, C. G. (2003). The evolution of lithospheric mantle beneath the Kalahari Craton and its margins. *Lithos*, 71(2–4), 215–241. <https://doi.org/10.1016/j.lithos.2003.07.006>
- Grove, T. L., & Parman, S. W. (2004). Thermal evolution of the Earth as recorded by komatiites. *Earth and Planetary Science Letters*, 219(3–4), 173–187. [https://doi.org/10.1016/s0012-821x\(04\)00002-0](https://doi.org/10.1016/s0012-821x(04)00002-0)
- Herzberg, C., Asimow, P. D., Arndt, N., Niu, Y., Leshner, C. M., Fitton, J. G., et al. (2007). Temperatures in ambient mantle and plumes: Constraints from basalts, picrites, and komatiites. *Geochemistry, Geophysics, Geosystems*, 8(2). <https://doi.org/10.1029/2006gc001390>
- Herzberg, C., Condie, K., & Korenaga, J. (2010). Thermal history of the Earth and its petrological expression. *Earth and Planetary Science Letters*, 292(1–2), 79–88. <https://doi.org/10.1016/j.epsl.2010.01.022>
- Hoare, B. C., Tomlinson, E. L., & Kamber, B. S. (2022). Evidence for a very thick Kaapvaal craton root: Implications for equilibrium fossil geotherms in the early continental lithosphere. *Earth and Planetary Science Letters*, 597, 117796. <https://doi.org/10.1016/j.epsl.2022.117796>
- Hoggard, M. J., Czarnota, K., Richards, F. D., Huston, D. L., Jaques, A. L., & Ghelichkhan, S. (2020). Global distribution of sediment-hosted metals controlled by craton edge stability. *Nature Geoscience*, 13(7), 504–510. <https://doi.org/10.1038/s41561-020-0593-2>
- Jaupart, C., Labrosse, S., Lucazeau, F., & Mareschal, J. C. (2007). 7.06-temperatures, heat and energy in the mantle of the earth. *Treatise on geophysics*, 7, 223–270.
- Jaupart, C., Mareschal, J. C., Guillou-Frotter, L., & Davaille, A. (1998). Heat flow and thickness of the lithosphere in the Canadian Shield. *Journal of Geophysical Research*, 103(B7), 15269–15286. <https://doi.org/10.1029/98jb01395>
- Kamber, B. S. (2010). Archean mafic–ultramafic volcanic landmasses and their effect on ocean–atmosphere chemistry. *Chemical Geology*, 274(1–2), 19–28. <https://doi.org/10.1016/j.chemgeo.2010.03.009>
- Kamber, B. S. (2015). The evolving nature of terrestrial crust from the Hadean, through the Archaean, into the Proterozoic. *Precambrian Research*, 258, 48–82. <https://doi.org/10.1016/j.precamres.2014.12.007>
- Kamber, B. S., & Tomlinson, E. L. (2019). Petrological, mineralogical and geochemical peculiarities of Archaean cratons. *Chemical Geology*, 511, 123–151. <https://doi.org/10.1016/j.chemgeo.2019.02.011>
- Keller, B., & Schoene, B. (2018). Plate tectonics and continental basaltic geochemistry throughout Earth history. *Earth and Planetary Science Letters*, 481, 290–304. <https://doi.org/10.1016/j.epsl.2017.10.031>
- Korenaga, J. (2006). Archean geodynamics and the thermal evolution of Earth. *Geophysical Monograph-American Geophysical Union*, 164, 7–32. <https://doi.org/10.1029/164gm03>
- Korenaga, J. (2008a). Urey ratio and the structure and evolution of Earth's mantle. *Reviews of Geophysics*, 46(2). <https://doi.org/10.1029/2007rg000241>
- Korenaga, J. (2008b). Plate tectonics, flood basalts and the evolution of Earth's oceans. *Terra Nova*, 20(6), 419–439. <https://doi.org/10.1111/j.1365-3121.2008.00843.x>
- Korenaga, J. (2018). Crustal evolution and mantle dynamics through Earth history. *Philosophical Transactions of the Royal Society A: Mathematical, Physical & Engineering Sciences*, 376(2132), 20170408. <https://doi.org/10.1098/rsta.2017.0408>
- Lenardic, A., Cooper, C. M., & Moresi, L. (2011). A note on continents and the Earth's Urey ratio. *Physics of the Earth and Planetary Interiors*, 188(1–2), 127–130. <https://doi.org/10.1016/j.pepi.2011.06.008>
- Lenardic, A., Moresi, L. N., & Mühlhaus, H. (2003). Longevity and stability of cratonic lithosphere: Insights from numerical simulations of coupled mantle convection and continental tectonics. *Journal of Geophysical Research*, 108(B6). <https://doi.org/10.1029/2002jb001859>
- Liu, Z., Ionov, D. A., Nimis, P., Xu, Y., He, P., & Golovin, A. V. (2022). Thermal and compositional anomalies in a detailed xenolith-based lithospheric mantle profile of the Siberian craton and the origin of seismic midlithosphere discontinuities. *Geology*, 50(8), 891–896. <https://doi.org/10.1130/g49947.1>

- Mather, K. A., Pearson, D. G., McKenzie, D., Kjarsgaard, B. A., & Priestley, K. (2011). Constraints on the depth and thermal history of cratonic lithosphere from peridotite xenoliths, xenocrysts and seismology. *Lithos*, 125(1–2), 729–742. <https://doi.org/10.1016/j.lithos.2011.04.003>
- McKenzie, D. (2020). Speculations on the generation and movement of komatiites. *Journal of Petrology*, 61(7), ega061. <https://doi.org/10.1093/ptrology/egaa061>
- McKenzie, D., & Bickle, M. J. (1988). The volume and composition of melt generated by extension of the lithosphere. *Journal of Petrology*, 29(3), 625–679. <https://doi.org/10.1093/ptrology/29.3.625>
- McKenzie, D., Jackson, J., & Priestley, K. (2005). Thermal structure of oceanic and continental lithosphere. *Earth and Planetary Science Letters*, 233(3–4), 337–349. <https://doi.org/10.1016/j.epsl.2005.02.005>
- McKenzie, D., & Priestley, K. (2008). The influence of lithospheric thickness variations on continental evolution. *Lithos*, 102(1–2), 1–11. <https://doi.org/10.1016/j.lithos.2007.05.005>
- Nesbitt, R. W., Jahn, B. M., & Purvis, A. C. (1982). Komatiites: An early Precambrian phenomenon. *Journal of Volcanology and Geothermal Research*, 14(1–2), 31–45. [https://doi.org/10.1016/0377-0273\(82\)90041-5](https://doi.org/10.1016/0377-0273(82)90041-5)
- Nickel, K. G., & Green, D. H. (1985). Empirical geothermobarometry for garnet peridotites and implications for the nature of the lithosphere, kimberlites and diamonds. *Earth and Planetary Science Letters*, 73(1), 158–170. [https://doi.org/10.1016/0012-821x\(85\)90043-3](https://doi.org/10.1016/0012-821x(85)90043-3)
- Nimis, P., & Grütter, H. (2010). Internally consistent geothermometers for garnet peridotites and pyroxenites. *Contributions to Mineralogy and Petrology*, 159(3), 411–427. <https://doi.org/10.1007/s00410-009-0455-9>
- Nimis, P., Preston, R., Perritt, S. H., & Chinn, I. L. (2020). Diamond's depth distribution systematics. *Lithos*, 376, 105729. <https://doi.org/10.1016/j.lithos.2020.105729>
- Nimis, P., & Taylor, W. R. (2000). Single clinopyroxene thermobarometry for garnet peridotites. Part I. Calibration and testing of a Cr-in-Cpx barometer and an enstatite-in-Cpx thermometer. *Contributions to Mineralogy and Petrology*, 139(5), 541–554. <https://doi.org/10.1007/s004100000156>
- Pearson, D. G., Canil, D., & Shirey, S. B. (2003). Mantle samples included in volcanic rocks: Xenoliths and diamonds. *Treatise on geochemistry*, 2, 568.
- Priestley, K., Ho, T., Takei, Y., & McKenzie, D. (2024). The thermal and anisotropic structure of the top 300 km of the mantle. *Earth and Planetary Science Letters*, 626, 118525. <https://doi.org/10.1016/j.epsl.2023.118525>
- Riel, N., Kaus, B. J., Green, E. C. R., & Berlie, N. (2022). MAGEMin, an efficient Gibbs energy minimizer: Application to igneous systems. *Geochemistry, Geophysics, Geosystems*, 23(7), e2022GC010427. <https://doi.org/10.1029/2022gc010427>
- Roberts, N. M., Condie, K. C., Palin, R. M., & Spencer, C. J. (2023). Hot, wide, continental back-arcs explain Earth's enigmatic mid-Proterozoic magmatic and metamorphic record. *Tektonika*, 1(1). <https://doi.org/10.55575/tektonika2023.1.1.32>
- Spencer, C. J., Mitchell, R. N., & Brown, M. (2021). Enigmatic mid-proterozoic orogens: Hot, thin, and low. *Geophysical Research Letters*, 48(16), e2021GL093312. <https://doi.org/10.1029/2021gl093312>
- Sudholz, Z. J., & Copley, A. C. (2024). Xenolith constraints on the mantle potential temperature and thickness of cratonic roots through time. *Zenodo*. [Dataset]. <https://doi.org/10.5281/zenodo.14376664>
- Sudholz, Z. J., Jaques, A. L., Yaxley, G. M., Taylor, W. R., Czarnota, K., Haynes, M. W., et al. (2023). Mapping the structure and metasomatic enrichment of the lithospheric mantle beneath the Kimberley Craton, Western Australia. *Geochemistry, Geophysics, Geosystems*, 24(9), e2023GC011040. <https://doi.org/10.1029/2023gc011040>
- Sudholz, Z. J., Yaxley, G. M., Jaques, A. L., & Brey, G. P. (2021). Experimental recalibration of the Cr-in-clinopyroxene geobarometer: Improved precision and reliability above 4.5 GPa. *Contributions to Mineralogy and Petrology*, 176(2), 1–20. <https://doi.org/10.1007/s00410-020-01768-z>
- Sudholz, Z. J., Yaxley, G. M., Jaques, A. L., Cooper, S. A., Czarnota, K., Taylor, W. R., et al. (2022). Multi-stage evolution of the South Australian craton: Petrological constraints on the architecture, lithology, and geochemistry of the lithospheric mantle. *Geochemistry, Geophysics, Geosystems*, 23(11), e2022GC010558. <https://doi.org/10.1029/2022gc010558>
- Szwilius, W., Afonso, J. C., Ebbing, J., & Mooney, W. D. (2019). Global crustal thickness and velocity structure from geostatistical analysis of seismic data. *Journal of Geophysical Research: Solid Earth*, 124(2), 1626–1652. <https://doi.org/10.1029/2018jb016593>
- Tang, M., Chu, X., Hao, J., & Shen, B. (2021). Orogenic quiescence in Earth's middle age. *Science*, 371(6530), 728–731. <https://doi.org/10.1126/science.abf1876>
- Tappe, S., Smart, K., Torsvik, T., Massuyeau, M., & de Wit, M. (2018). Geodynamics of kimberlites on a cooling Earth: Clues to plate tectonic evolution and deep volatile cycles. *Earth and Planetary Science Letters*, 484, 1–14. <https://doi.org/10.1016/j.epsl.2017.12.013>
- Taylor, W. (1998). An experimental test of some geothermometer and geobarometer formulations for upper mantle peridotites with application to the thermobarometry of fertile lherzolite and garnet websterite. *Neues Jahrbuch für Mineralogie - Abhandlungen*, 172(2–3), 381–408. <https://doi.org/10.1127/njma/172/1998/381>
- Tomlinson, E. L., & Holland, T. J. (2021). A thermodynamic model for the subsolidus evolution and melting of peridotite. *Journal of Petrology*, 62(1), egab012. <https://doi.org/10.1093/ptrology/egab012>
- Walter, M. J. (1998). Melting of garnet peridotite and the origin of komatiite and depleted lithosphere. *Journal of Petrology*, 39(1), 29–60. <https://doi.org/10.1093/ptroj/39.1.29>
- Weller, O. M., Copley, A., Miller, W. G. R., Palin, R. M., & Dyck, B. (2019). The relationship between mantle potential temperature and oceanic lithosphere buoyancy. *Earth and Planetary Science Letters*, 518, 86–99. <https://doi.org/10.1016/j.epsl.2019.05.005>
- Ziberna, L., Nimis, P., Kuzmin, D., & Malkovets, V. G. (2016). Error sources in single-clinopyroxene thermobarometry and a mantle geotherm for the Novinka kimberlite, Yakutia. *American Mineralogist*, 101(10), 2222–2232. <https://doi.org/10.2138/am-2016-5540>